

The Optimum Number of OSPF Areas for MANETs¹

Jangeun Jun² and Mihail L. Sichitiu
Department of Electrical and Computer Engineering
North Carolina State University
Raleigh, NC 27695-7911
email: {jjun, mlsichit}@ncsu.edu

Hector D. Flores and Stephan J. Eidenbenz
Discrete Simulation Science, CS-5
Los Alamos National Laboratory
Los Alamos, NM 87545
email: {hflores, eidenben}@lanl.gov

Abstract—Mobile ad hoc networks (MANETs) are a critical technology in filling the gap where the network infrastructure is insufficient or does not exist at all. The dynamic topology of MANET requires relatively large control overhead which impedes the scalability of the network. Recently, adapting a widely-used Internet protocol such as Open Shortest Path First (OSPF) for MANETs has been actively investigated to benefit from its maturity, interoperability, and scalability. To enhance the scalability of OSPF, several extensions have been proposed including flooding backbone, differential hellos, smart peering, and distance effect. However, most of the existing work is based on the assumption of single OSPF area. In this paper, we present promising results from employing multiple OSPF areas as an efficient mean to enhance the scalability of MANETs. A novel analytical model is developed to capture the relationship between the number of areas and the flooding overhead. We perform theoretical analysis to show that there exists an optimum number of areas that minimizes the overhead. By using areas, the overhead can be significantly reduced (in some cases by 95%). The analytical results are verified with detailed simulation experiments. Finally, several candidate dynamic area formation schemes are investigated with different mobility models. The results show that the optimum number of areas has an even greater impact on the scalability of the scenarios with higher degree of realism.

I. INTRODUCTION

Over the last decade, mobile ad hoc networks (MANETs) have been an area of active research. The origin of MANETs dates back to the advent of military packet radio networks in 1960s. With the unprecedented

advancement in mobile devices and wireless communication technologies, MANETs are rapidly expanding applications in commercial and military environments. MANET is considered especially important for situations with sparse or inexistent infrastructure. Recently, wireless ad hoc networks showed their potential to fill the gap for the Internet, landline telephone, and cellular services in disaster areas [1].

A. Scalability and Routing Overhead

In MANETs, due to node mobility and wireless links, the topology of the network dynamically changes at much higher rate than conventional wired/wireless networks. The topological instability can be counteracted by spending more control packets (e.g., more frequently flooded updates). However, considering the limited wireless bandwidth, a good MANET routing scheme should reduce the overhead as much as possible to allow the network to scale to a large number of nodes.

Many schemes have been proposed for enhancing the scalability of MANETs by reducing the overhead without compromising the performance (i.e., route correctness). Fisheye State Routing (FSR) [2] is a link state routing protocol designed for MANETs. In contrast to the conventional full flooding, it improves scalability by providing more frequent updates the the nodes closer to the origin of the update. Optimized Link State Routing (OLSR) [3] is another link state routing scheme for MANETs that reduces flooding overhead by allowing only a subset of nodes to participate in flooding. Other schemes contain the flooding overhead within a certain cluster [4] or hierarchical boundary [5]. In on-demand (or reactive) protocols such as AODV [6], route discovery packets are flooded only when necessary. DSR [7] is also an on-demand protocol that uses aggressive caching to reduce unnecessary flooding. If available, location

¹This work was supported by the Center for Advanced Computing and Communication at NCSU.

²Jangeun Jun, a Ph.D student from North Carolina State University performed part of this research at Los Alamos National Laboratory as a summer intern student.

information is considered as an efficient means ([8], [9]) to increase scalability by suppressing the network-wide flooding. In ZRP [10], very similar to the concept of OSPF areas, the MANET is split into *zones* and a (proactive) intra-zone and a (reactive) inter-zone routing protocols are proposed.

B. Adapting OSPF for MANETs

Recently, adapting a widely-used Internet protocol such as Open Shortest Path First (OSPF) to MANET environment has been actively investigated as an efficient way to enhance the scalability [11].

While the baseline OSPF provides sophisticated functionalities such that the protocol can be directly used for MANETs with minor extensions like defining new interface type [11], it requires relatively large amount of overhead compared to the protocols dedicated for MANETs. The large overhead is a serious problem because frequent changes of the topology will cause an implosion of flooded link state updates, which takes away user bandwidth and thus, impedes the scalability of the protocol.

The origin of OSPF overheads can be attributed to the three subprotocols and five different types of OSPF packets. Periodic hello packets are generated by the hello protocol. Database description (DBDesc), link state request (LSR), link state update (LSU), and link state acknowledgement (LSAck) packets are used by the synchronization protocol. The flooding protocols also uses the LSU packets to propagate link state advertisements (LSAs).

To achieve overhead efficiency of OSPF, various extensions have been proposed. One of the most commonly explored approaches is to reduce the number of the OSPF routers that participate in the flooding. Both the MANET Designated Routers (MDR) [12] and the Multi-Point Relays [13] extensions choose a connected dominating set (CDS) where only the nodes in the resulting CDS will perform flooding. They use different topology reduction algorithms (MDR is source-independent and MPR is source-dependent) to form a flooding backbone. The simulation study on the two schemes reported in [14] shows that both schemes reduce a significant amount of overhead without compromising the routing/forwarding performance.

In addition to reducing the number of flooding nodes, reducing the size of each hello packet and formation of adjacencies are proposed. In differential hellos scheme, the size of the hello packet is minimized by including only new information (i.e., newly added or lost neigh-

bors) in the periodic hello transmission. In Smart Peering algorithm [15], the reachability information available in the SPT is used to reduce the number of adjacencies without compromising reachability and routing paths redundancy.

In contrast to the schemes that reduce the overhead by employing flooding backbone or selective peering, the notion of *distance effect* is explored in the overhead reduction scheme proposed in [16]. In the distance effect scheme, whether to relay (or relood) a link state update (LSU) at each node is determined by the hop-count distance the LSU traveled from the originating node (similar to what can be inferred from the TTL field in the IP packet header). As a result, the frequency of reflooding is attenuated as the LSU travels farther from the origination. The simulation results show that the scheme provides significant overhead reduction without compromising the packet delivery performance.

C. Gap and Contribution

Although the proposed extensions provide efficient overhead reduction for MANETs, all of them are based on the assumption that only a single OSPF area exists in the network. We focus on the fact that the baseline OSPF already supports hierarchical topologies with multiple OSPF areas. With proper extensions to the embedded multiple-area feature of OSPF, we can enhance the scalability of the protocol in a MANET environment. To the best of authors' knowledge, this capability has not yet been explored as a means to reduce the overhead and to enhance the scalability.

Multiple areas may reduce the flooding overhead. Flooding will be contained in each area as far as the change (mainly due to mobility) does not affect the route calculation at the nodes in other areas. However, a mobile node may cross the area border and as a result, the event has to be updated in all the areas including the two areas the node just left and entered. With increased number of areas for the given network, the range of intra-area flooding will be decreased. However, on the other hand, the frequency that a mobile node crosses the area border (which will trigger network-wide flooding) increases with the increased number of areas. This trade-off between the number of areas and the total flooding overhead raises a key question about the ideal number of areas for any given network. If the number of areas is resolved, the network can be partitioned into multiple areas to maximize the scalability.

This paper presents theoretical and simulation results from using multiple OSPF areas in MANETs. An ana-

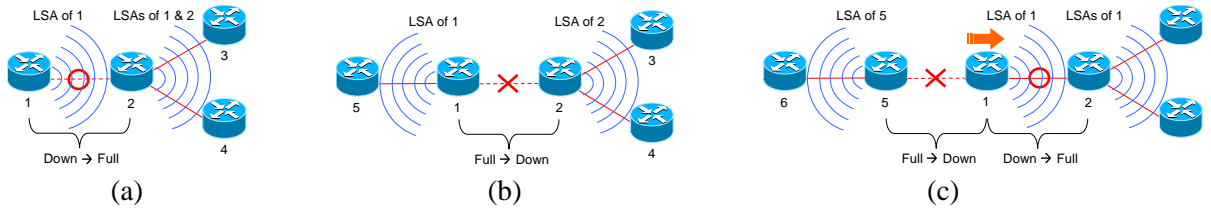


Fig. 1. Origination of flooding due to different events: (a) a node comes up and establishes adjacency, (b) neighbor relationship breaks down between two nodes, and (c) neighbor relationship change by mobility.

lytical model is developed to investigate the scalability performance of multiple OSPF areas in MANETs. We perform theoretical analysis based on the model and show that there exists an optimum number of areas that minimizes the overhead. The theoretical result is verified with detailed simulation experiments. By using areas, for medium (over 100 nodes) to large (over 1000 nodes) networks, the overhead can be reduced to as low as 5% of the single-area case. We extend our investigation for the area formation and maintenance schemes. Several candidate schemes are investigated with different mobility models. The results show that the optimum number of areas is a critical scalability factor for the scenarios with realistic mobility model and dynamic partitioning of areas.

II. MODEL

In this section, we look into the flooding mechanism of OSPF protocol and establish an analytical model that will be used to evaluate the impact of multiple areas on flooding overhead.

A. Origin of Flooding

We define some important elements in the modeling of OSPF flooding. First, we define the term “topology”. In general, topology is described as the configuration of a communication network or the method in which nodes of a network are connected by links. In terms of protocol layering stack, topology can be defined at different layers. For wireless networks, it is often defined as physical-layer connectivity among wireless nodes which is again determined by the signal reception range. Sometimes MAC-layer compatibility is considered together with physical-layer. In our study, topology is considered mainly at the network layer, and it is defined by OSPF routers and their relationship in terms of OSPF neighbor state. For example, two OSPF routers with different area IDs cannot become neighbors even if they are within the signal range. More precisely, it is an undirected graph where vertices represent OSPF routers, and an edge represents fully adjacent neighbor relationship between

two routers. All the terms used in graph theory may apply to the OSPF topology under consideration. For convenience, nodes and links will be interchangeably used for vertices and edges, respectively.

To estimate and measure the effect of topology changes on the OSPF flooding overhead, there should be an objective view on the origin of topology changes. Here, transient effects such as temporal fading are not considered as the source of topology changes. The topology in our study is defined by OSPF routers and their neighbor states, and thus, such transient events at the physical layer will be automatically filtered out by periodically transmitted hello packets and associated time-outs. Three major events that contribute to topology changes can be summarized as: (a) when a node comes up and starts transmitting hellos and establishes neighbor relationship through synchronization with adjacent nodes, (b) a node goes down and stops transmitting hellos and as a result, existing full adjacency with each neighbor is torn down, and (c) a node moves from one place to another and stops receiving hellos from the old neighbors and starts receiving hellos from new nodes, each causing break down and establishment of neighbor relationship with old and new neighbors, respectively.

Any of these events affects the topology by changing the OSPF neighbor state between the node that causes the event and its neighbor. In steady state analysis, where all the nodes converge and share a common view on the network, the main contributor to the topology change will be mobility of the nodes. The atomic (i.e., the smallest scale) topology change involves two nodes and one link between them. Therefore, the origin of topology change should be viewed as creation or destruction of a link. However, a neighbor event (either entering or leaving full state) always involves two nodes and it is indeed these two nodes that generate the router-LSAs (link state advertisements) to be flooded.

In our study, mobility causes neighbor state changes, where each neighbor event triggers two nodes to initiate LSA flooding. We assume all the events occur sequen-

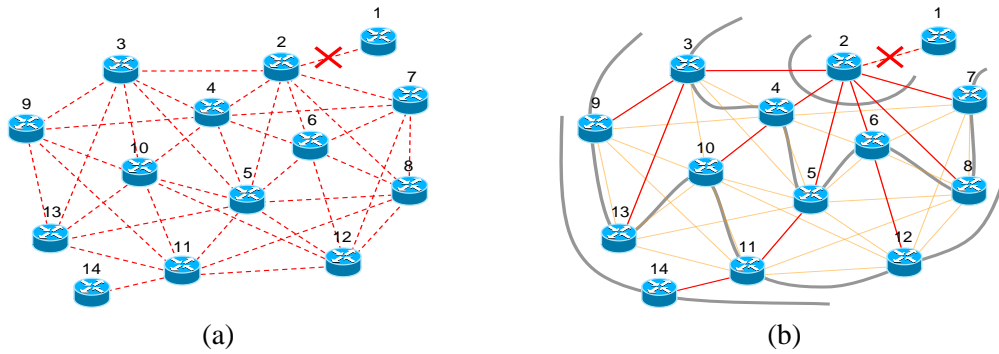


Fig. 2. How LSAs are flooded in an area: (a) initial topology and (b) spanning-tree propagation of the first LSAs.

tially, i.e., although a moving node leaves the reception range of its neighbor nodes almost at the same time, the loss of the node will be detected at different time due to jitter in hello transmission and associated router-dead time-out.

Figure 1 depicts flooding origination caused by different events. In Fig. 1-(a), node-1 comes up and establishes adjacency with node-2. Although both nodes-1 and 2 experience neighbor state change, since node-1 is a leaf node that just came up, the LSAs of both nodes are flooded towards node-3 and 4 (of course node-2's LSA reaches node-1 as well). In Fig. 1-(b), node-1 and 2 tear down the neighbor relationship after the link is disconnected. This neighbor state change triggers both node-1 and 2 to originate flooding. In Fig. 1-(c), node-1 moves from one position to another, tearing down the neighbor relationship with node-5 and establishing with node-2. In this case, two neighbor state changes occur and thus, four LSAs are originated. Each of node-5 and 2 generates one LSA, indicating the loss and discovery of node-1, respectively. Two LSAs are generated by node-1, one for the loss of node-5 and the other for the discovery of node-2. Note that in Fig. 1-(a) and (c), node-2's LSA will also reach node-1, but it is not shown to avoid cluttering the illustration.

B. Estimation of Flooding per Neighbor State Change

To derive the formula that provides the amount of LSA flooding induced by a neighbor state change, we first define following variables:

- $F \equiv$ total number of flooded LSAs per neighbor state change in the area.
- $n \equiv$ total number of OSPF nodes in the area.
- $L \equiv$ total number of leaf nodes in the area.
- $I \equiv$ total number of nodes that are isolated from the origin of flooding.

Figure 2 depicts how LSAs are flooded in an area. The initial topology is shown in Fig. 2-(a). In Fig. 2-

(b), the neighbor state change between node-1 and 2 triggers LSA flooding throughout the area. In Fig. 2-(b), red solid lines represent the first LSA to arrive at each node, forming a spanning tree rooted at node-2. The spanning tree can be different depending on the jitter at each node. The LSA originated by node-2 will first reach nodes-3, 4, 5, 6, 7 and 8. Grey curve represents a contour line where nodes have the same hop-count distance from the origin.

Although nodes-9, 10, 11, 12, and 13 appear as the leaves of the spanning tree in Fig. 2-(b), their degrees are greater than one as shown in the original topology in Fig. 2-(a). These nodes participate in flooding when receiving an LSA because they have neighbors other than the one that sent the first LSA. On the contrary, node-14 is a leaf node that has no other neighbors to relay the received LSA. Thus, it does not participate in flooding. Finally, node-1 is isolated from the origin of flooding and thus, it does not take part in the flooding. Therefore, the total number of LSA-floodings induced by single neighbor state change can be generalized as:

$$F = n - L - I \quad [LSAs]. \quad (1)$$

Applying (1) to Fig. 2 yields $F = 14 - 1 - 1 = 12$.

By choosing reasonably high enough node density, we can assume that the network graph is connected within the area even after one edge is disconnected. This assumption will also eliminate the existence of a leaf node as shown in Fig. 2-(b). Note that if the network is connected after the neighbor state change, two different LSAs will be originated at both ends of the origin edge. Therefore, by assuming that the area is 2-edge-connected, we can rewrite (1) as:

$$F = 2 \times n \quad [LSAs]. \quad (2)$$

If nodes-1 and 7, and nodes-13 and 14 are connected in Fig. 2, the network satisfies the connectivity assumption, resulting in the total flooding as $F = 2 \times 14 = 28$.

Assuming C number of neighbor state changes (i.e., deletion of old neighbors and/or addition of new neighbors) experienced by one mobile node during the time duration of t , flooding rate of the network F_R can be derived from (2) as:

$$F_R = \frac{2nMC}{t} = 2nMR \text{ [LSAs/s]}, \quad (3)$$

where M is the number of mobile nodes and $R = \frac{C}{t}$.

C. Estimation of Neighbor State Changes

Neighbor state changes are important because they are the origin of flooding as discussed in the previous section. Figure 3 illustrates the estimation of neighbor changes. In Fig. 3-(a), the relation between node degree (i.e., the number of full state neighbors) and the average node density is depicted. The shaded circle represents the signal reception range of node-1. All the nodes within the circle are assumed to establish full adjacency with node-1, and thus, the number of node-1's neighbors is 10. In general, the degree (or neighbor density) of a node n_D can be described as:

$$n_D = A_C \delta - 1 = \pi r^2 \delta - 1 \text{ [Neighbors/Node]}, \quad (4)$$

where A_C is the area of the signal range and r is the radius of the signal range. The average node density δ is defined as:

$$\delta = \frac{n}{S} = \frac{n}{l^2} \text{ [Nodes/m}^2\text{]}, \quad (5)$$

where, n is the total number of nodes in the network, S is the total area (including all the OSPF areas if the network has multiple areas), and $S = l^2$. We assume that the nodes are uniformly distributed in the network.

Figure 3-(b) shows the estimation of the amount of neighbor changes when node-1 moves from position X to Y. Node-1 moves d [m] at the velocity of v [m/s]. Along with node-1's movement, some new neighbors are added and some are deleted. The total number of newly discovered neighbors by the time node-1 reaches position Y pertains to the shaded area in Fig. 3-(b). Likewise, the total number of the deleted neighbors pertains to the same area because the area covered by the range of node-1 is symmetrical. Therefore, the sum of the added and deleted neighbors (i.e., the total number of neighbor state changes) C can be written as:

$$C = 2(A_S \delta - 1) = 4rd\delta - 2, \quad (6)$$

where A_S is the shaded area. From this result, (3) can be rewritten as:

$$F_R = \frac{2nMC}{t} = \frac{4nM(2rd\delta - 1)}{t} \text{ [LSAs/s]}, \quad (7)$$

As we will focus on the flooding overhead per mobile node as a function of the expected distance a node travels at one leg, from (7), we define $F(d)$ as follows:

$$F(d) = 4n(2rd\delta - 1) \text{ [LSAs/Leg]}. \quad (8)$$

Figure 3-(c) considers the case where node-1 makes a turn. Node-1 moves from position X to Y, and then Y to Z. If the total distance in Fig. 3-(c) is the same as (b) (i.e., $d_1 + d_2 = d$), and the velocity is constant (i.e., $v_1 = v_2 = v$), then the resulting calculation of F_R for Fig. 3-(c) is the same as (b). To allow our model to be amenable to analysis, we do not consider the boundary condition where node-1 bounces on the border of the terrain.

III. ANALYSIS

In this section, the analysis of the relationship between the flooding overhead and node mobility is presented.

A. Mobility Model and Expected Traveling Distance

The expected traveling distance of a mobile node is important because the induced flooding overhead will be proportional to the distance. For the analysis, the network is assumed to be partitioned into one or more OSPF areas based on geographical location of each node. Mobility of a node will contribute to flooding overhead in two ways:

- by causing neighbor state changes within the area it travels,
- and by leaving the old area and joining a new area (i.e., crossing the area border).

The former is handled by the intra-area routing and the latter by the inter-area routing of OSPF. We define the number of LSAs created by the former F and the latter F_A where the suffix A indicates the flooding of LSAs caused by multiple "area" configuration. Note that F is a function of the traveling distance of the mobile node, and F_A is a function of the number of area borders crossed by the node. We define the former independent variable as distance d and the latter as inter-area distance d_A , where suffix A indicates distance between two "areas".

$$F = f(d) \text{ [LSAs]}, \quad (9)$$

$$F_A = g(d_A) \text{ [LSAs]}. \quad (10)$$

In legacy OSPF, summary-LSAs are generated by area border routers (ABRs) for the destinations outside the area. For MANETs, unless a proprietary address assignment scheme is employed, nodes are assumed to have unique addresses which cannot be aggregated

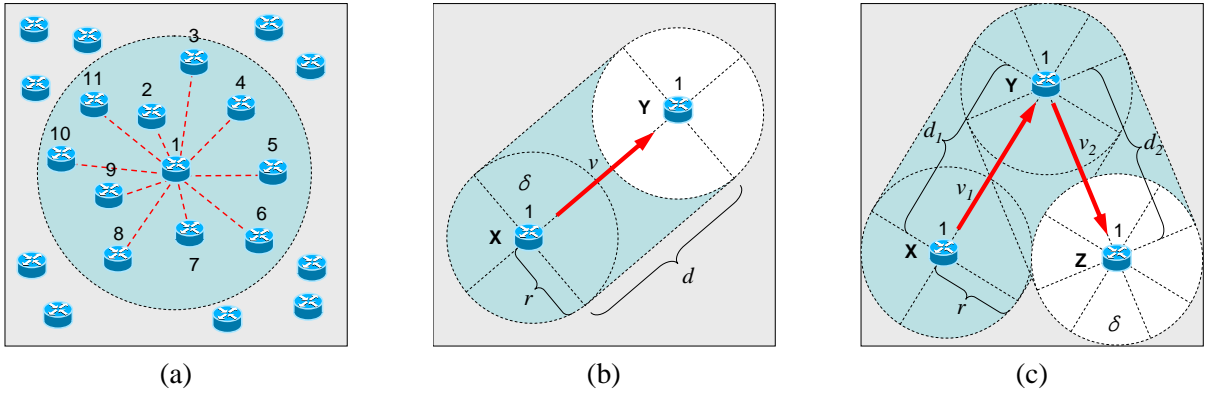


Fig. 3. Estimation of neighbor state changes: (a) average node degree and node density, (b) neighbor changes from node mobility, and (c) neighbor changes and change of movement direction.

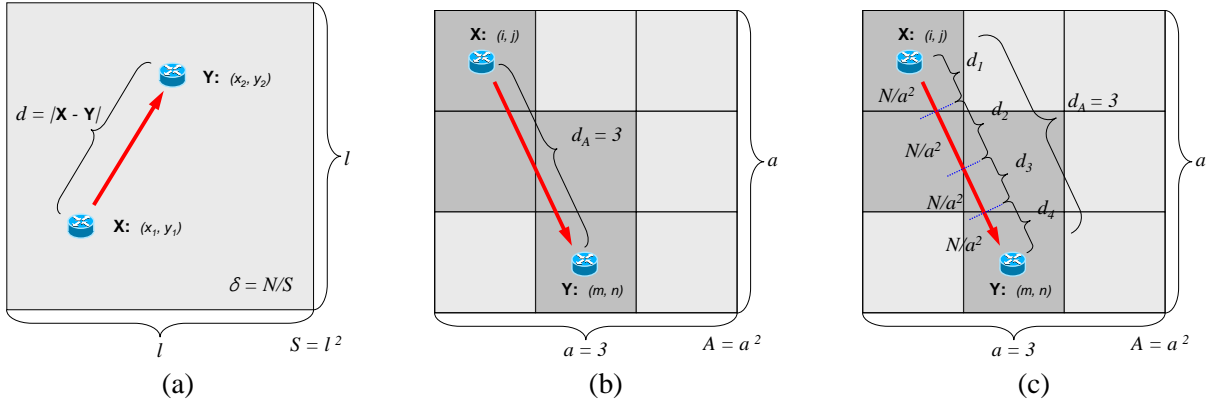


Fig. 4. Analysis of distance traveled by a mobile node: (a) intra-area distance is measured in the Euclidean space R^2 , (b) inter-area distance is measured as area-count between two end areas, and (c) the effect of both intra- and inter-area distance.

TABLE I
EXPECTED VALUE OF INTRA-AREA DISTANCE $E(d_A)$ AS A FUNCTION OF THE NUMBER OF AREAS a .

a	1	2	3	4	5	6	7	8	9	10	11	12
$E(d_A)$	0	1	1.778	2.5	3.2	3.889	4.571	5.25	5.926	6.6	7.273	7.944

at ABRs. Thus, two summary-LSAs are generated by each ABR and flooded by intra-area routers when a node crosses the area border: One LSA advertising the departure of the node from the old area and the other advertising the arrival at the new area. Here, since ABRs of the two areas (old and new) do not flood the summary-LSAs that they originated into their own areas, each summary-LSA gets flooded in $A - 1$ areas, where A is the number of areas in the network. Therefore, the total number of inter-area LSAs induced by a mobile node that crosses area borders d_A times can be written as:

$$F_A = 2d_A \left(\frac{A-1}{A} \right) n = 2d_A \left(1 - \frac{1}{a^2} \right) n \quad [LSAs]. \quad (11)$$

The mobility model assumed for the derivation is a special case of the random waypoint model and it can

be described as follows:

- At each leg, from the position $X(x_1, y_1)$, it chooses a random destination $Y(x_2, y_2)$.
- The destination coordinate variables x_2 and y_2 are selected from a uniform distribution of $(0, l)$.
- The node moves from position X to Y at a constant velocity, and there is no pause time.

Based on the mobility model, we first derive the expected value of intra-area distance d . Figure 4-(a) shows the traveled distance by a node in the area of $S = l^2$.

$$E(d) = \int_l \int_l \int_l \int_l d(x_1, x_2, y_1, y_2) p_d dx_1 dy_1 dx_2 dy_2, \quad (12)$$

where $d(x_1, x_2, y_1, y_2)$ and p_d are:

$$d(x_1, x_2, y_1, y_2) = \sqrt{(x_1 - x_2)^2 + (y_1 - y_2)^2}, \quad (13)$$

$$p_d = \frac{1}{S^2} = \frac{1}{l^4}. \quad (14)$$

Equation (12) is a special case of the problem of evaluating the average distance in arbitrary bounded regions. The closed form solution for (12) is known as:

$$E(d) = \alpha l, \quad (15)$$

where $\alpha = \frac{2+\sqrt{2}+5\ln(1+\sqrt{2})}{15} \cong 0.521405433$.

Now, we turn to inter-area distance d_A . Figure 4-(b) shows the traveled inter-area distance by a node in the network of nine areas (i.e., $A = a^2 = 9$). In this case, the node crosses area borders three times and thus, $d_A = 3$. Since our mobility model assumes uniform distribution in choosing the destination, the expected value of the inter-area distance d_A can be described as follows:

$$E(d_A) = \sum_{i=1}^a \sum_{j=1}^a \sum_{m=1}^a \sum_{n=1}^a \frac{1}{A^2} D_A(X, Y), \quad (16)$$

where $X : (i, j)$ and $Y : (m, n)$ indicate the leaving and arriving areas in the form of a matrix. The area at the top left of the terrain is identified as area $(1, 1)$ and the one at the bottom right as (a, a) . $D_A(X, Y)$ represents the inter-area distance d_A between two specific areas $X : (i, j)$ and $Y : (m, n)$, and it is defined as follows:

$$D_A(X, Y) = |i - m| + |j - n|. \quad (17)$$

By applying (17) to (16), we can derive $E(d_A)$ as a function of the square root of the number of areas ($= a$) as:

$$\begin{aligned} E(d_A) &= \sum_{i=1}^a \sum_{j=1}^a \sum_{m=1}^a \sum_{n=1}^a \frac{1}{a^4} (|i - m| + |j - n|) \\ &= \frac{2}{a^2} \sum_{i=1}^a \sum_{m=1}^a |i - m| = \frac{2(a+1)(a-1)}{3a} \end{aligned} \quad (18)$$

Table I shows the resulting $E(d_A)$ for increasing a . For single area (i.e. $a = 1$), mobile nodes will never cross the area border, which is shown as $E(d_A) = 0$. For four-area configuration (i.e., $a = 2$), it is expected that a mobile node will cross one area border per leg on the average.

Note that for $a > 3$, there exist areas that do not share any area border with the backbone area. In legacy OSPF, all the areas are expected to be connected to the backbone area, forming a spoke topology around the backbone. Otherwise, they should be connected to the backbone via

virtual links. In our study, instead of proposing a specific scheme to connect remote areas to the backbone area, we assume that all the areas are somehow connected to the backbone area. This assumption does not compromise the analysis of impact of multiple areas on flooding overhead.

IV. THE OPTIMUM NUMBER OF AREAS

In this section, the optimum number of areas of a given network is obtained by combining all the results from analysis and it is verified using both computation and simulation.

A. Analytical Results

The total number of flooded LSAs in the network is the sum of both intra-area and inter-area LSAs. We define Φ as:

$$\Phi = F + F_A \quad [LSAs]. \quad (19)$$

Since (8) assumes single area network, n should be replaced by n/a^2 for multiple areas, and d should be partitioned into multiple segments as d_1, \dots, d_k , where $k = d_A + 1$. Figure 4-(c) presents the relationship among d , k , and d_A . By (5) and (15), F can be rewritten as follows:

$$\begin{aligned} F &= 4 \frac{n}{a^2} (2rd_1\delta - 1) + \dots + 4 \frac{n}{a^2} (2rd_k\delta - 1) \\ &= 4 \frac{n}{a^2} (2rd\delta - 1) = \frac{4n}{a^2} \left(\frac{2\alpha r n}{l} - 1 \right) \quad [LSAs]. \end{aligned} \quad (20)$$

Turning to the total number of inter-area LSAs, (11) can be rewritten after applying the result from (18) as follows:

$$F_A = \frac{4(a+1)^2(a-1)^2}{3a^3} n \quad [LSAs]. \quad (21)$$

Finally, from (20) and (21), (19) can be described as a function of a and n :

$$\Phi(a, n) = \frac{8\alpha r}{a^2 l} n^2 + \frac{4(a^4 - 2a^2 - 3a + 1)}{3a^3} n \quad [LSAs], \quad (22)$$

where α is the constant parameter for the expected traveling distance $E(d)$, l is the length of one side of square terrain, r is the signal reception range, a^2 is the number of the OSPF areas, and n is the total number of nodes in the network.

The result of (22) shows that the number of LSAs grows as $O(n^2)$ where n is the total number of nodes. Note that this result represents the induced LSAs for one mobile node. Thus, it holds for the case where the number of mobile nodes is constant. If the number of mobile nodes is given as a certain fraction of the total

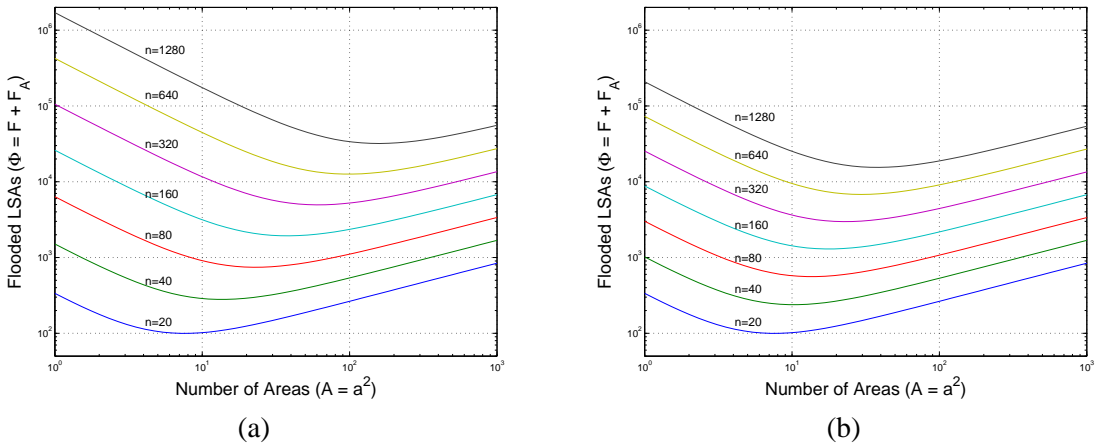


Fig. 5. The number of flooded LSAs for the varied number of areas ($A = a^2$) and number of nodes (n): (a) when the area of the network is constant ($S = l^2 = 1 \text{ km}^2$) and (b) when the node density is constant ($\delta = 20 \text{ nodes/km}^2$).

number of nodes (e.g., 10 % of all the nodes are mobile), the number of induced LSAs will grow as $O(n^3)$.

Figure 5 shows the number of flooded LSAs as a function of the number of areas ($A = a^2$) and the number of nodes. In Fig. 5-(a), the area of the network is constant ($S = l^2 = 1 \text{ km}^2$) while the node degree grows with increasing number of nodes. In Fig. 5-(b), the node density is constant ($\delta = 20 \text{ nodes/km}^2$) while the network size grows with increasing number of nodes. Signal range r is 250 m. For fair comparison, both Fig. 5-(a) and (b) are given the same scale for y-axis.

Figure 5 proves that the maximum flooding reduction can be achieved by choosing appropriate number of areas for the given network. As the number of areas is increased in both Fig. 5-(a) and (b), the number of flooded LSAs decreases due to the “isolating” effect of areas where intra-area flooding involves $\frac{n}{A}$ nodes in each area. However, if A is increased beyond saturation point, the inter-area flooding will prevail, and eventually will increase the overall flooding overhead. We define the area number that provides the maximum flooding reduction as “optimum area number”. It can be noted from the comparison of Fig. 5-(a) and (b) that for the same number of nodes, the optimum area number is larger for denser networks.

The number of areas strongly influences the overhead. As shown in Fig 5-(b), for a network of 1280 nodes with the average node density of 20 nodes/km^2 , the overhead can be reduced to 10%. If the node density is scaled with the number of nodes, Fig 5-(a) shows even greater overhead reduction (around 3%).

The optimum number of areas can be obtained by finding the natural number that is the closest to the

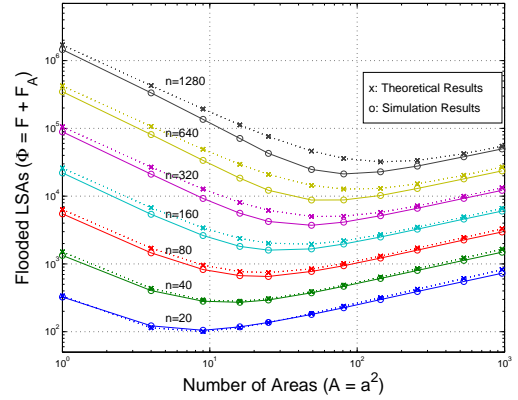


Fig. 6. The comparison of the results from simulation and computation: the number of flooded LSAs with regard to the increased number of areas ($A = a^2$) and number of nodes (n) when the area of the network is constant ($S = l^2 = 1 \text{ km}^2$).

solution of:

$$\frac{\partial \Phi(a, n)}{\partial a} = 0, \quad (23)$$

which leads to the following equation:

$$\frac{(a^4 + 2a^2 + 6a - 3)}{a} = \beta, \quad (24)$$

where $\beta = \frac{12\alpha rn}{l}$. For example, if $n = 320$, $r = 250 \text{ m}$, and $l = 1000 \text{ m}$, the optimum number of areas can be obtained from (24) as $A = 64$ (or $a = 8$). Since the left-hand side of (24) monotonically increases for $a > 0$, it can be inferred that the optimum number of areas grows with the node density and decreases with the dimensions of terrain.

B. Simulation Results

The theoretical results are verified with detailed simulation experiments. Since there is no simulator that

supports multiple OSPF areas to the best of the authors' knowledge, a customized simulator is developed such that the overhead generation events of OSPF protocol is precisely captured in the scenarios with multiple areas and node mobility [17]. Simulation was performed with different number of nodes (from 20 to 1280) and areas. Simulation for each scenario is run for one hour and the result is averaged after 30 repetitions. The terrain is a square with area of 1km^2 and the mobile node follows random waypoint model with constant velocity of 10m/s and zero pause time. The total number of LSAs are measured with regard to the increased number of areas. Figure 6 shows the comparison of the theoretical and simulation results. The overall simulation result closely matches the theoretically estimated values. The simulation results are sometimes lower than the theoretical estimations. This is because the model used in the theoretical analysis does not take into account the *boundary effect*. When the mobile node is close to a terrain border or an area border, the minimum number of neighbors will be a half (when the mobile is close to the middle of the border) or a quarter (when the mobile is close to the corner) of normal situation. This effect becomes more significant for a large number of nodes and multiple areas. If the node density is constant (i.e. network terrain size is fixed) with increased number of nodes and areas, the size of each area will shrink and thus, the A_C value in (4) as illustrated in Fig. 3 will decrease (because the neighborhood indicated by A_C is not a disk any more). For this reason, the theoretical estimation tend to over-estimated the overhead for a large number of nodes and areas, and this can be verified from the curves shown in Fig. 6. For medium to small number of nodes, the boundary effect is not so conspicuous. Overall, the optimum number of areas from the theoretical estimation is close to the simulation result.

V. AREA FORMATION AND MAINTENANCE

In the previous sections, we showed that using the optimum number of areas can significantly reduce the overhead. This result will naturally lead to the question of how to *automatically and dynamically* establish and maintain such multiple areas. To make the problem amenable to analysis, we assumed a simple mobility model and a regular grid partitioning of areas such that a network in a square terrain is partitioned into a^2 number of square areas. Obviously, such assumptions may not hold in real situations because the shape of the network its areas will be irregular depending on the topology, and the mobility will be fairly different from the random

waypoint model. Therefore, to shed light on the effect of dynamic area formation scheme and mobility model on the overhead reduction performance, conceivable area formation schemes are investigated under different mobility models.

In real life scenarios, it can be efficient to map the area of a node to its physical location. For example, the whereabouts of a node will be highly correlated to a room, building, campus, district, or city. The topology change can be contained within each area if the area of a node is resolved by its location. One of the strengths of this approach is that it requires minimal computation and protocol complexity in the area formation and maintenance. Although it requires location information at each node, with the advancement in positioning solutions including both GPS and GPS-less technologies, relatively accurate location information will not be that expensive to afford in near future. We call this approach *Geographical Partitioning (GP)*. In many cases, the boundary between the geographically-derived areas can be unclear. The notion of activity points (e.g., center of a downtown square) can be more realistic in such a case. A node will resolve its area identity by selecting the closest activity point. By doing this, each node does not have to know the exact shape of the irregular areas. The resulting layout of area assignment will be a Voronoi diagram with the activity points around the center of each polygon cell. We call this scheme *Realistic Partitioning (RP)*. In contrast to the GP and RP schemes, a distributed partitioning algorithm that provides the minimum edge cut and balanced vertices can be realistic for the situation where location information is unavailable [18], [19]. We call this approach *Topological Partitioning (TP)* because the partitioning is done based on the topology of the network. An important drawback is that each node should know the global topology on which it will run the partitioning algorithm to resolve its area.

Figure 7 shows the scalability performance of the potential schemes compared through simulation experiments. Simulation parameters are similar to Section IV-B except that we used Realistic Synthetic Mobility (RSM) model in addition to the Random Waypoint (RWP) model. RSM model is produced from the synthetic pedestrian movement data of the Rice University campus. One of the important properties of this model [20], [21] is spatial-temporal correlation in node mobility. The model provides high level of realism which is lacking in the variations of random waypoint model. The measurement unit is changed from $[\Phi/\text{node}/\text{leg}]$ to $[\Phi/\text{s}]$ because the RSM does not have legs as RWP

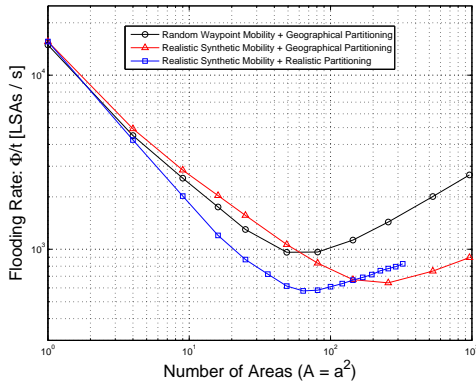


Fig. 7. Comparison of flooding rates for different mobility models and area partitioning schemes.

does. There are 320 mobile nodes in each scenario. For fair comparison, the velocity of RWP is adjusted such that all the models generate the same overhead for the single-area case. In Fig. 7, the result from RWP and GP is similar to what is shown in Fig. 6. The combination of RSM and GP outperforms RWP and GP, but RSM requires a large number of areas. This is due to the irregular node distribution in RSM where many grid areas are wasted without containing any node. The most realistic scenario (i.e., RSM and RP) shows the maximum overhead reduction with the smallest number of areas because nodes tend to gather around each activity point that serves as a reference for the area identity. The maximum number of areas in RSM and RP is lower than others due to the limited activity points in the RSM model. Overall, the optimum number of areas shows greater impact on the scalability for more realistic scenarios.

VI. CONCLUSION

This paper provides promising results for using multiple OSPF areas for scalable MANETs. A novel analytical model is presented to capture the effect of multiple OSPF areas. The theoretical and simulation results show that there exists an optimum number of areas and that it plays a critical role in the scalability. We also present several potential area formation and maintenance schemes. The findings from the study of the optimum number of areas can be applied to other existing table-driven protocols - especially to the link state routing protocols including OLSR and OSPF extensions (MPR, MDR, or distance effect) as the overhead reduction from using an optimum number of areas is independent of such single-area approaches.

REFERENCES

- [1] "Hurricane Katrina reveals strengths of emerging technologies," *IEEE IT Professional*, vol. 7, Sep 2005.
- [2] M. G. G. Pei and T. Chen, "Fisheye state routing: A routing scheme for ad hoc wireless networks," in *Proc. of ICC 2000*, (New Orleans, LA), June 2000.
- [3] T. Clausen and P. Jacquet, "Optimized link state routing protocol (OLSR)." RFC 3626, Oct. 2003.
- [4] C. Chiang, H. K. Wu, W. Liu, and M. Gerla, "Routing in clustered multihop mobile wireless networks with fading channel," in *Proc. of IEEE Singapore International Conference on Networks*, 1997.
- [5] K. Xu and M. Gerla, "A heterogeneous routing protocol based on a new stable clustering scheme," in *Proc. of the Military Communications Conference (MILCOM)*, (Anaheim, CA), Oct. 2002.
- [6] C. Perkins, E. Belding-Royer, and S. Das, "Ad hoc on-demand distance vector (AODV) routing." RFC 3561, July 2003.
- [7] D. B. Johnson and D. A. Maltz, "Dynamic source routing in ad hoc wireless networks," in *Mobile Computing* (Imielinski and Korth, eds.), vol. 353, Kluwer Academic Publishers, 1996.
- [8] Y. B. Ko and N. H. Vaidya, "Location aided routing (LAR) in mobile ad hoc networks," *Wireless Networks*, vol. 6, pp. 307–321, Sept. 2000.
- [9] S. Basagni, I. Chlamtac, V. Syrotiuk, and B. Woodward, "A distance routing effect algorithm for mobility (DREAM)," in *Proc. of ACM Mobicom '98*, (Dallas, TX), pp. 76–84, Oct. 1998.
- [10] Z. Haas, "A new routing protocol for the reconfigurable wireless networks," in *Proc. of the IEEE Int. Conf. on Universal Personal Communications*, Oct. 1997.
- [11] F. Baker, M. Chandra, R. White, J. Macker, T. Henderson, and E. Baccelli, "Problem statement for OSPF extensions for mobile ad hoc routing." draft-baker-manet-ospf-problem-statement-00, Sep. 23 2003.
- [12] R. Ogier and P. Spagnolo, "MANET extensions of OSPF using CDS flooding." Internet Draft draft-ogier-manet-ospf-extension-04, Jul 2005.
- [13] M. Chandra, "Extensions to OSPF to support mobile ad hoc networking." Internet Draft draft-chandra-ospf-manet-ext-03, Apr 2005.
- [14] T. R. Henderson, P. A. Spagnolo, and G. Pei, "Evaluation of OSPF MANET extensions." Boeing Technical Report, Jul. 21 2005.
- [15] A. Roy, "Adjacency reduction in OSPF using SPT reachability." Internet Draft draft-roy-ospf-smart-peering-00, Jan 2006.
- [16] Jangeun Jun and Mihail L. Sichitiu, "Scalable OSPF updates for MANETs," in *Proc. of the IEEE Globecom 06 - WASNet*, Nov 2006.
- [17] "OASISv1.0: OSPF Areas Simulation System, Version 1.0." <http://www4.ncsu.edu/~jjun/oasis1.0.zip>, Jul 2006.
- [18] M. E. J. Newman, "Detecting community structure in networks," *Eur. Phys. J. B*, no. 38, pp. 321–330, 2004.
- [19] L. Danon, J. Duch, A. Diaz-Guilera, and A. Arenas, "Comparing community structure identification," *J. Stat. Mech.*, p. P09008, 2005.
- [20] S. Eidenbenz, H. Flores, N. Hengartner, and R. Riedi, "Describing MANETS: Principal component analysis of sparse mobility traces," in *Proc. of PE-WASUN'06 (to appear)*, Oct. 2006.
- [21] H. Flores, S. Eidenbenz, N. Hengartner, and R. Riedi, "PedSims: Building towards realism of mobility models for wireless networks," in *(submitted)*, 2006.